Supplemental Material

Ionic strength effect on regulating the synthetic assemble of polyoxometalate clusters with slow magnetic relaxation behaviors

Jing Cai,*[a] Run Ye,[a] Xinhao Liu,[b] Leilei Guo,[a] Xinrong Qiao*[a]

[a]College of biology and pharmaceutical engineering, Xinyang Agriculture and Forestry University, Xinyang, Henan, 464000, China

[b]Department of central laboratory, Xinyang Agriculture and Forestry University, Xinyang, Henan, 464000, China

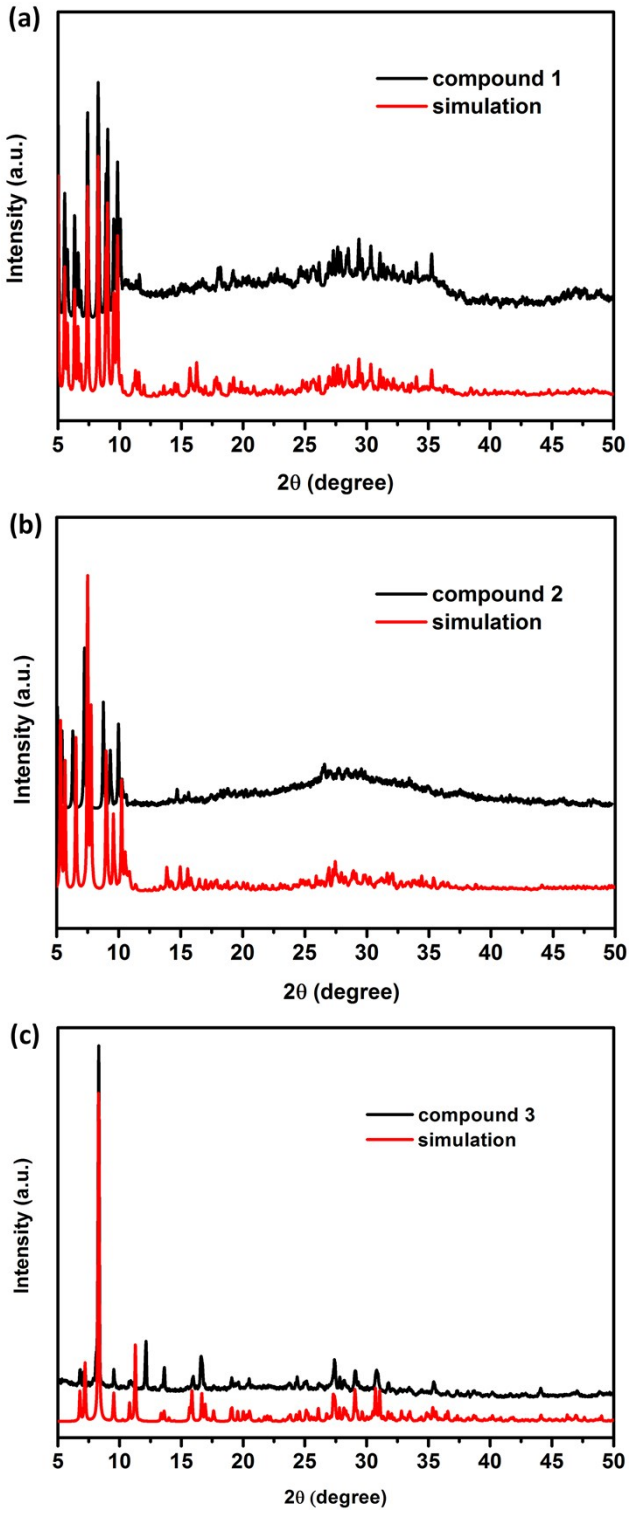

Fig. S1. Powder X-ray diffraction patterns for compounds **1-3**.

The PXRD patterns of compounds **1-3** were investigated, and the most peak positions of simulated were in good agreement with the experimental patterns, respectively, indicating the good phase purity of the products.

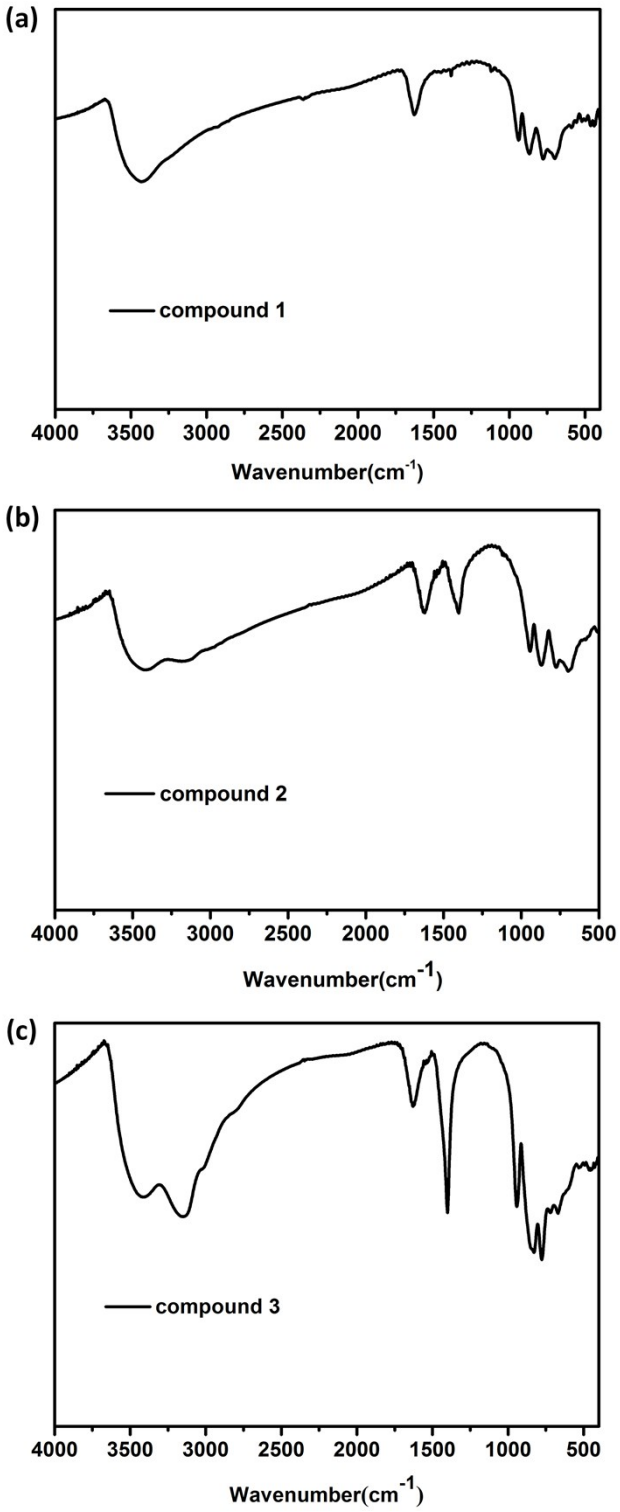

Fig. S2. Infrared spectra of compounds **1-3**.

The IR spectra of **1-3** were measured in the range of 4000 – 400 cm^{-1}. The broad band around 3420 cm^{-1} can be deemed as characteristic peaks of the lattice and coordinated water molecules, while **2** and **3** appear two peaks between 3100 and 3420 cm^{-1} that are probably associated with the stretching vibration of N-H except for the

stretching vibration of O-H. Peaks at about 1630 cm^{-1} may be ascribed to the in-plane bending vibration of water molecules. The feature peaks of 945, 870, 775, 701, 506, 445 cm^{-1} for **1**, 947, 873, 773, 698, 512, 461 cm^{-1} for **2** and 941, 828, 777, 669, 433 cm^{-1} for **3** in the fingerprint region can be regarded as the stretching vibration of W-O_d, W-O_b-W, W-O_c-W, and Sb-O_a in polyoxoanion framework.

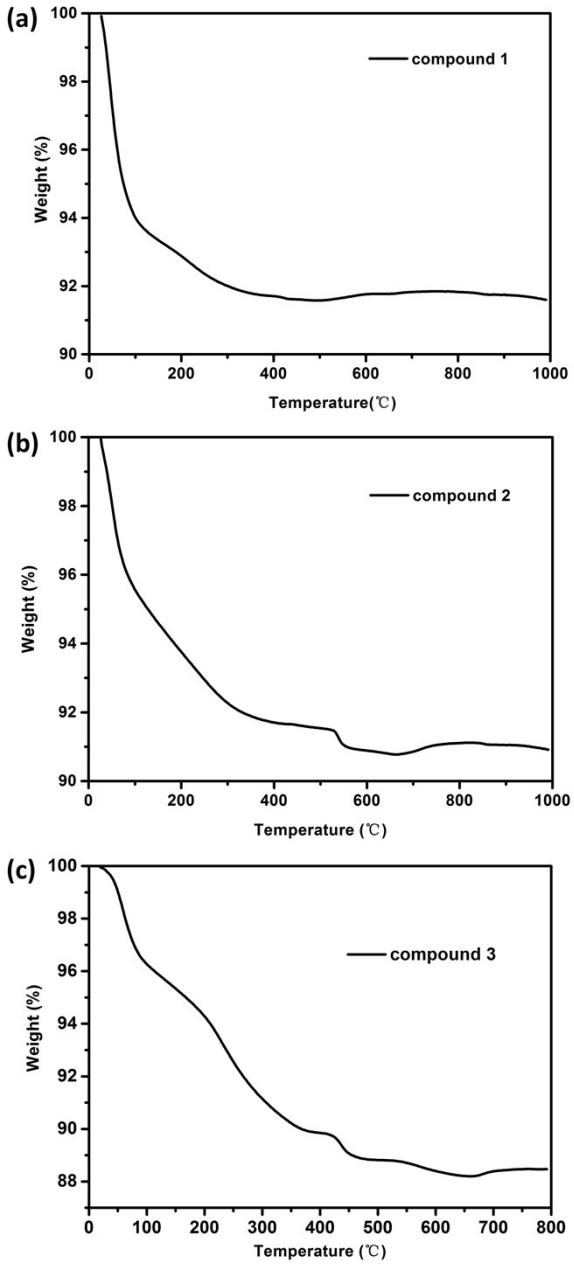

Fig. S3. TG analysis of compounds **1-3** .

The TG curves of compounds **1-3** were shown in Figure S3, the weight loss of 6.3% from 20 to 200 °C for **1**, 8.5% from 20 to 500 °C for **2** and 9.2% from 20 to 400 °C

for **3** can be ascribed to the removal of the guest and coordinated water molecules. Among them, the weight loss of **1** and **2** are less than their theoretical values 9.7% and 10.6% possibly because that **1** and **2** are easy efflorescence to lose part of crystalline water molecules. The slow mass loss in the temperature range of 200-500 °C, 500-660 °C and 400-650 °C for **1-3** correspond to the slow decomposition of compounds. The unusual increase of TGA curves after 500, 660 and 650 °C for **1-3** can be attributed to the valence conversion from Sb^{III} to Sb^{V}. The final residue of **1** is 91.6%, which agrees with calculated value 90.0% based on Dy_2O_3, NiO, Sb_2O_5, Na_2O and WO_3. For **2**, the final residue is 91.1%, which agrees with calculated value 88.8% based on Dy_2O_3, Sb_2O_5, Na_2O and WO_3. For **3**, the final residue is 88.5%, which agrees with calculated value 87.2% based on NiO, Sb_2O_5, Na_2O and WO_3.

Table S1. Crystallographic Data for Compounds **1-3**

Compound	**1**	**2**	**3**
Formula	$H_{104}Na_{10}K_{10}Sb_3Dy_3NiW_{30}O_{162}$	$H_{134}N_5Na_8K_4Sb_4Dy_3W_{30}O_{167}$	$H_{96}N_9NaSb_2Ni_2W_{20}O_{100}$
Mr	9744.28	9707.05	5883.46
Crystal system	triclinic	monoclinic	monoclinic
Space group	*P*-1	*C*2/*c*	*C*2/*m*
a/Å	18.2445(6)	35.159(3)	17.8033(14)
b/Å	19.9956(7)	18.5597(7)	18.5672(16)
c/Å	24.4742(6)	48.357(3)	14.1660(12)
α/°	93.078(2)	90	90
β/°	99.426(2)	114.193(9)	113.239(9)
γ/°	116.645(3)	90	90
V/Å^3	7790.2(5)	28784(4)	4302.8(7)
Z	2	8	1
T/K	186	191	178
ρ_{calc}g/cm^3	3.829	4.168	4.203
μ/mm^{-1}	24.339	26.985	27.761
F(000)	7742.0	31039.0	4684.0
2θ/°	5.858-50	5.706-50	6.156-49.996
Observed reflections	18376	25278	3883
Data/parameters	27383/1784	25278/1789	3883/270
GOF	1.002	1.086	1.088
$R_1[I > 2\sigma(I)]$	0.0832	0.1059	0.0678
wR_2(All data)	0.1928	0.2022	0.1689

[a] $R_1=\sum||F_O| - |F_C||/\sum|F_O|$; [b] $wR_2=\{\sum[w(F_O^2 - F_C^2)^2]/\sum[w(F_O^2)^2]\}^{1/2}$

Table S2. Selected bond distances of **1**

Dy1—O19	2.401 (19)	Ni1—O127	2.024 (18)
Dy1—O36	2.263 (18)	Sb1—O107	1.987 (19)
Dy1—O35	2.417 (17)	Sb1—O101	1.963 (15)
Dy1—O22	2.20(2)	Sb1—O102	2.03 (2)
Dy1—O103	2.30 (2)	Sb2—O119	2.003 (18)
Dy1—O20	2.37 (3)	Sb2—O53	1.979 (16)
Dy1—O21	2.37 (3)	Sb2—O50	1.932 (17)
Dy2—O30	2.308 (18)	Sb3—O122	1.986 (17)
Dy2—O111	2.409 (19)	Sb3—O94	2.016 (16)
Dy2—O146	2.319 (16)	Sb3—O79	1.95 (2)
Dy2—O110	2.431 (16)	W1—O69	1.744 (18)
Dy2—O62	2.413 (19)	W1—O34	1.98 (2)
Dy2—O141	2.44 (2)	W1—O110	1.98 (2)
Dy2—O63	2.551 (19)	W1—O62	2.204 (17)
Dy2—O86	2.40 (2)	W1—O108	1.736 (18)
Dy2—O31	2.591 (18)	W1—O63	2.091 (16)
Dy3—O48	2.431 (18)	W2—O111	1.98 (2)
Dy3—O68	2.29 (2)	W2—O113	1.695 (16)
Dy3—O139	2.40 (2)	W2—O62	2.143 (18)
Dy3—O66	2.32 (2)	W2—O65	1.771 (19)
Dy3—O65	2.199 (19)	W2—O31	2.38 (2)
Dy3—O60	2.31 (2)	W2—O22	1.79 (2)
Dy3—O64	2.51 (3)	W3—O111	2.10 (2)
Dy3—O61	2.70 (3)	W3—O112	1.729 (17)
Ni1—O69	2.05 (2)	W3—O124	1.886 (19)
Ni1—O112	2.12 (2)	W3—O110	1.972 (19)
Ni1—O113	2.058 (15)	W3—O141	2.148 (17)
Ni1—O114	2.04 (2)	W3—O85	1.70 (2)
Ni1—O59	1.98 (2)		

Table S3. Selected bond distances of **2**

Dy1—O102	2.46 (3)	Sb2—O88	1.99 (3)
Dy1—O96	2.64 (3)	Sb3—O116	2.00 (3)
Dy1—O51	2.42 (3)	Sb3—O117	1.99 (2)
Dy1—O50	2.43(2)	Sb3—O109	2.04 (3)
Dy1—O103	2.49 (3)	Sb4—O74	2.09 (3)
Dy1—O5	2.56 (3)	Sb4—O77	1.97 (2)
Dy1—O6	2.35 (3)	Sb4—O72	2.10 (3)
Dy1—O111	2.37 (3)	Sb4—O78	2.02 (3)
Dy1—O49	2.17 (3)	Sb4—O75	2.00 (3)
Dy2—O87	2.46 (3)	Sb4—O79	1.95 (3)
Dy2—O32	2.40 (3)	W1—O102	2.08 (2)
Dy2—O36	2.41 (3)	W1—O51	1.95 (3)
Dy2—O94	2.14 (3)	W1—O142	1.73 (3)
Dy2—O160	2.30 (2)	W1—O75	1.81 (3)
Dy2—O34	2.46 (5)	W1—O5	2.16 (4)
Dy2—O35	2.53 (7)	W1—O25	1.96 (2)
Dy2—O33	2.40 (5)	W2—O96	2.13 (3)
Dy3—O143	2.35 (3)	W2—O97	1.87 (3)
Dy3—O90	2.36 (3)	W2—O51	2.00 (2)
Dy3—O99	2.42 (3)	W2—O50	2.15 (2)
Dy3—O56	2.35 (3)	W2—O77	1.81 (3)
Dy3—O91	2.37 (3)	W2—O52	1.81 (3)
Dy3—O76	2.16 (3)	W3—O102	1.94 (2)
Dy3—O89	2.41 (3)	W3—O50	2.03 (2)
Sb1—O81	1.93 (3)	W3—O74	1.83 (3)
Sb1—O83	1.98 (2)	W3—O76	1.79 (3)
Sb1—O82	1.96 (3)	W3—O94	1.90 (3)
Sb2—O105	1.96 (2)	W3—O103	2.24 (3)
Sb2—O23	2.02 (3)		

Table S4. Selected bond distances of **3**

Ni1—O4[3]	2.17 (3)	W1—O4AA	1.86 (2)
Ni1—O2W	2.09 (3)	W1—O4AA[2]	1.86 (2)
Ni1—O2W[1]	2.09 (3)	W1—O2	1.981 (16)
Ni1—O1W	2.10 (4)	W1—O2[2]	1.981 (16)
Ni1—O18[1]	2.141 (19)	W4—O5	2.27 (2)
Ni1—O18	2.141 (19)	W4—O3	1.766 (17)
Sb1—O5	1.98 (2)	W4—O3[1]	1.766 (17)
Sb1—O20[1]	2.020 (16)	W4—O6[1]	2.071 (18)
Sb1—O20	2.020 (16)	W4—O6	2.071 (18)
W1—O3	2.091 (17)	W4—O4	1.74 (2)
W1—O3[2]	2.091 (17)		

Symmetry transformations used to generate equivalent atoms: #1 +*x*, 1-*y*, +*z*; #2 +*y*, −*x*+1, 1-*z*; #3 1-*y*, −*x*+1, 1-*z*

Table S5. The valence state results of W atoms from $\{W_3O_{11}\}$ unit, Sb, Dy and Ni for

compound **1** based on BVS.

atoms		length (Å)	BVS
W1	O69	1.744	5.999
	O34	1.98	
	O110	1.98	
	O62	2.204	
	O108	1.736	
	O63	2.091	
W2	O111	1.98	6.388
	O113	1.695	
	O62	2.143	
	O65	1.771	
	O31	2.38	
	O22	1.79	
W3	O111	2.10	6.540
	O112	1.729	
	O124	1.886	
	O110	1.972	
	O141	2.148	
	O85	1.70	
Ni	O69	2.05	2.097
	O112	2.12	
	O113	2.058	
	NO114	2.04	
	O59	1.98	
	O127	2.024	
Sb1	O107	1.987	2.847
	O101	1.963	
	O102	2.03	
Sb2	O119	2.003	3.023

	O53	1.979	
	O50	1.932	
Sb3	O122	1.986	2.920
	O94	2.016	
	O79	1.95	
Dy1	O19	2.401	2.924
	O36	2.263	
	O35	2.417	
	O22	2.20	
	O103	2.30	
	O20	2.37	
	O21	2.37	
Dy2	O30	2.308	2.901
	O111	2.409	
	O146	2.319	
	O110	2.431	
	O62	2.413	
	O141	2.44	
	O63	2.551	
	O86	2.40	
	O31	2.591	
Dy3	O48	2.431	2.956
	O68	2.29	
	O139	2.40	
	O66	2.32	
	O65	2.199	
	O60	2.31	
	O64	2.51	
	O61	2.70	

Table S6. The valence state results of W atoms from $\{W_3O_{11}\}$ unit, Sb and Dy for compound **2** based on BVS.

atoms		length (Å)	BVS
W1	O102	2.08	5.960
	O51	1.95	
	O142	1.73	
	O75	1.81	
	O5	2.16	
	O25	1.96	
W2	O96	2.13	5.700
	O97	1.87	
	O51	2.00	
	O50	2.15	
	O77	1.81	
	O52	1.81	
W3	O111	2.10	6.555
	O112	1.729	
	O124	1.886	
	O110	1.972	
	O141	2.148	
	O85	1.70	
Sb4	O74	2.09	4.893
	O77	1.97	
	O72	2.10	
	O78	2.02	
	O75	2.00	
	O79	1.95	
Sb1	O81	1.93	3.140
	O83	1.98	
	O82	1.96	

Sb2	O105	1.96	2.872
	O23	2.02	
	O88	1.99	
Sb3	O116	2.00	2.719
	O117	1.99	
	SO109	2.04	
Dy1	O102	2.46	2.982
	O96	2.64	
	O51	2.42	
	O50	2.43	
	O103	2.49	
	O5	2.56	
	O6	2.35	
	O111	2.37	
	O49	2.17	
Dy2	O87	2.46	2.962
	O32	2.40	
	O36	2.41	
	O94	2.14	
	O160	2.30	
	O34	2.46	
	O35	2.53	
	O33	2.40	
Dy3	O143	2.35	2.831
	O90	2.36	
	O99	2.42	
	O56	2.35	
	O91	2.37	
	O76	2.16	
	O89	2.41	

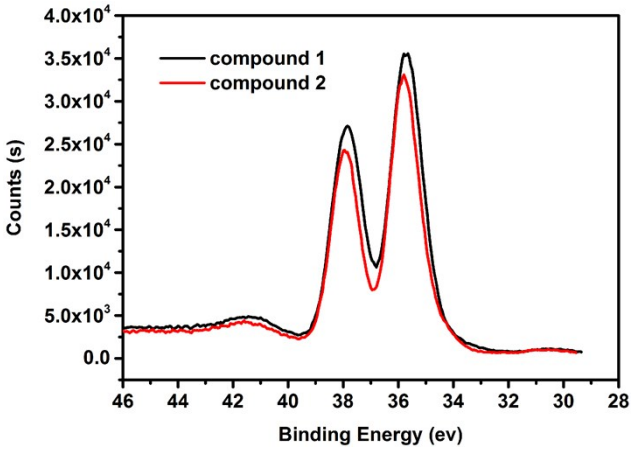

Fig. S4. The XPS spectra of W atoms for compounds **1** and **2**.

As shown in Figure S4, the XPS results of W atoms for **1** and **2** exhibit similar behaviors. The peaks around 37.85 and 35.65 eV for **1** and around 37.95 and 35.80 eV for **2** correspond to the W $4f_{5/2}$ and W $4f_{7/2}$ of the W^{6+} centers.[1]

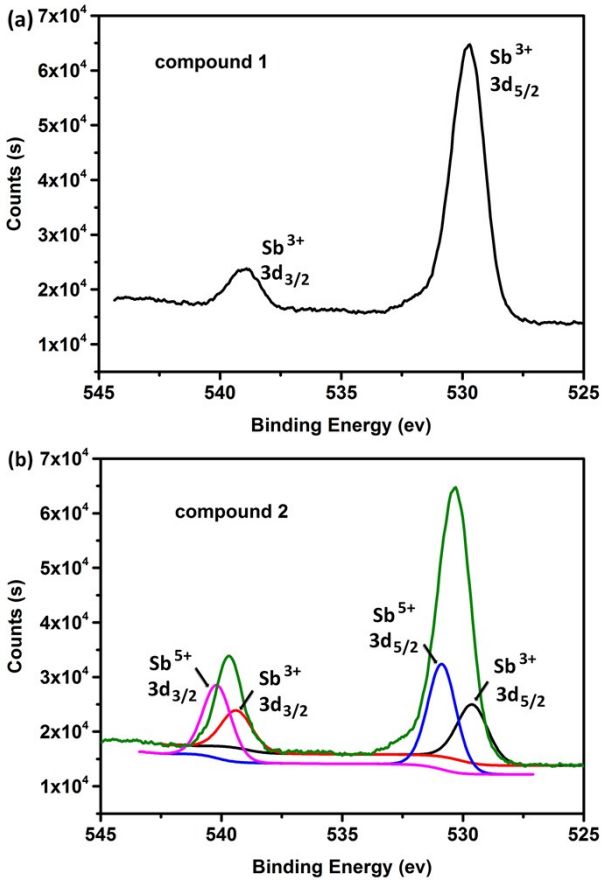

Fig. S5. The XPS spectra of Sb atoms for compounds **1** and **2**.

As shown in Figure S4a, the signals at 529.7 and 538.9 eV for **1** are ascribed to the Sb $3d_{5/2}$ and Sb $3d_{3/2}$ of the Sb^{3+} cations. As for **2**, both the Sb $3d_{3/2}$ and Sb $3d_{5/2}$ spectra can be divided into two characteristic peaks. And four deconvoluted peaks were observed in the Sb 3d region at 540.2, 530.9, 539.4 and 529.65 eV, confirming the Sb valence states as Sb^{5+} and Sb^{3+}.[2]

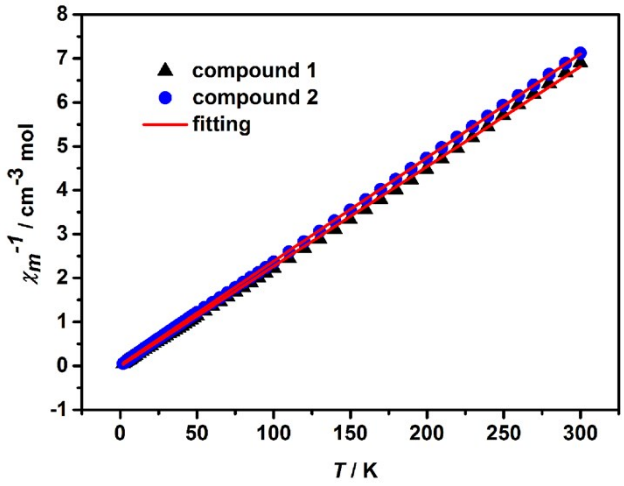

Fig. S6. Plots of $1/\chi_m$ *vs*. T to a Curie-Weiss law for compounds **1** and **2** in the range of 2-300 K.

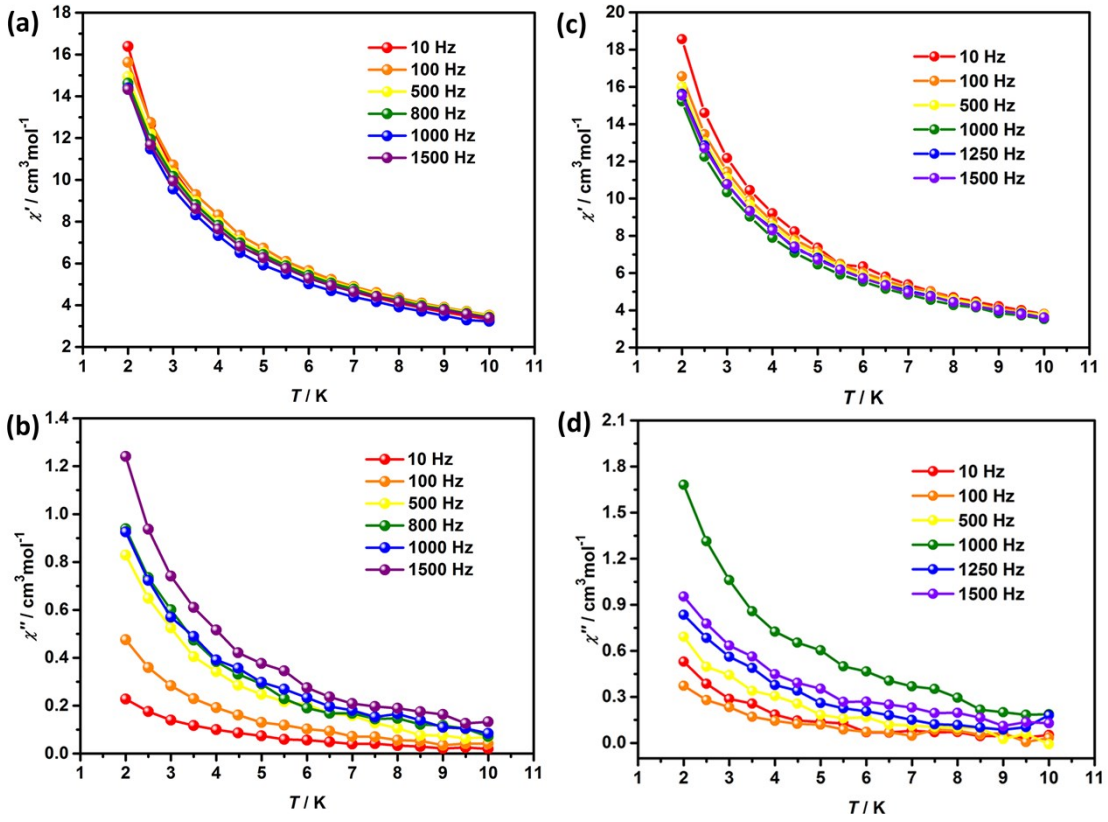

Fig. S7. Temperature dependence of in-phase (χ′) (a), (c) and out-of-phase (χ″) (b), (d) of ac susceptibility signals at different frequencies under a zero dc feld for **1** and **2**.

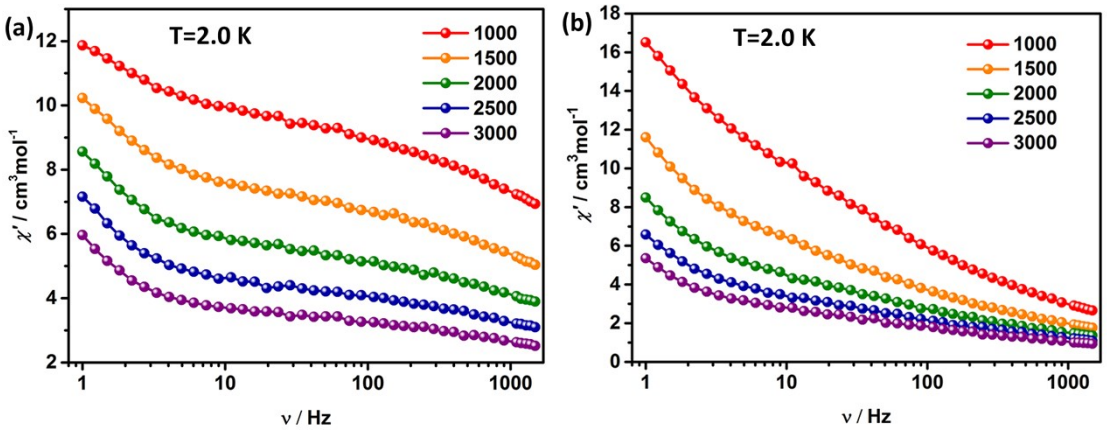

Fig. S8. Field dependence of in-phase (χ′) of ac susceptibility signals at 2 K for **1** (a) and **2** (b).

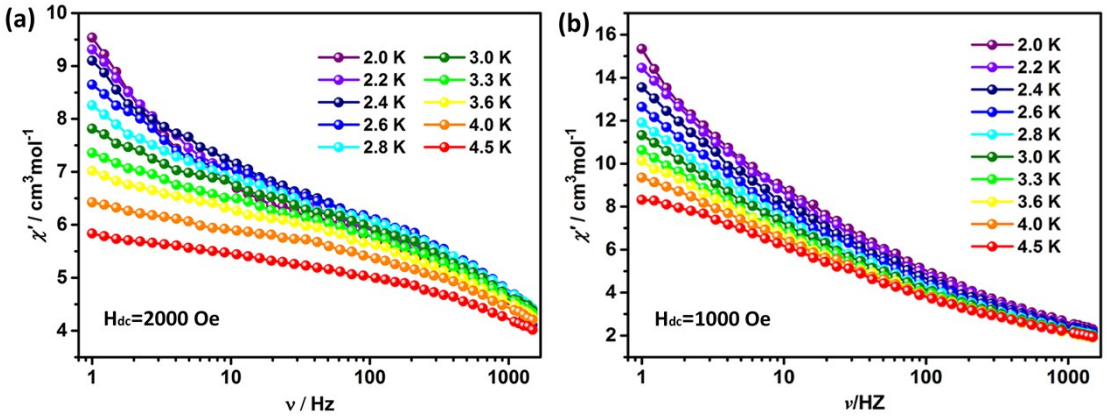

Fig. S9. Temperature dependence of in-phase (χ′) of ac susceptibility signals at 2 K for **1** (a) and **2** (b).

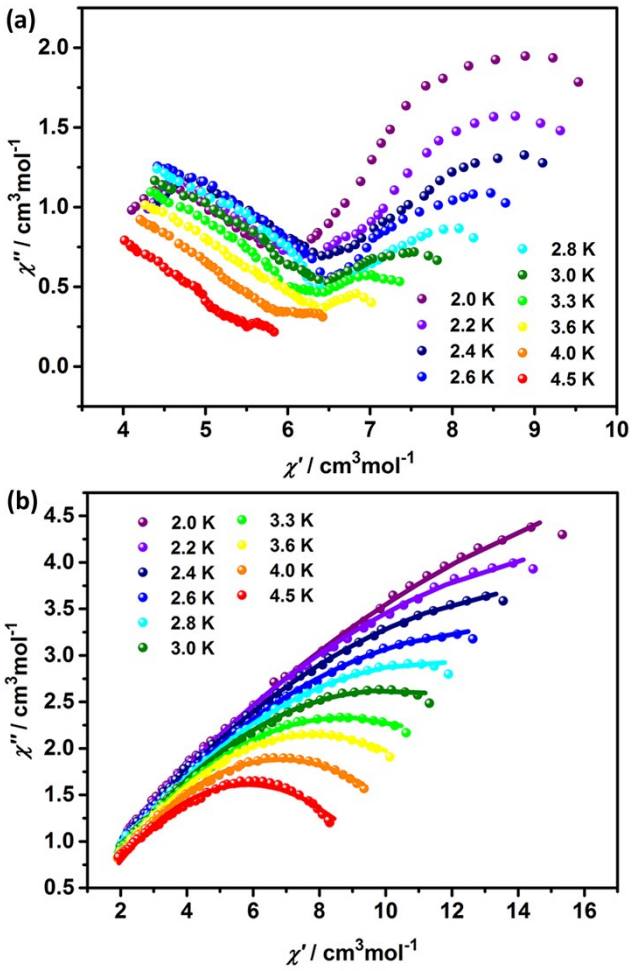

Fig. S10. Cole-Cole diagrams of **1** (a) and **2** (b) with the solid lines represent the best fits to the experimental data.

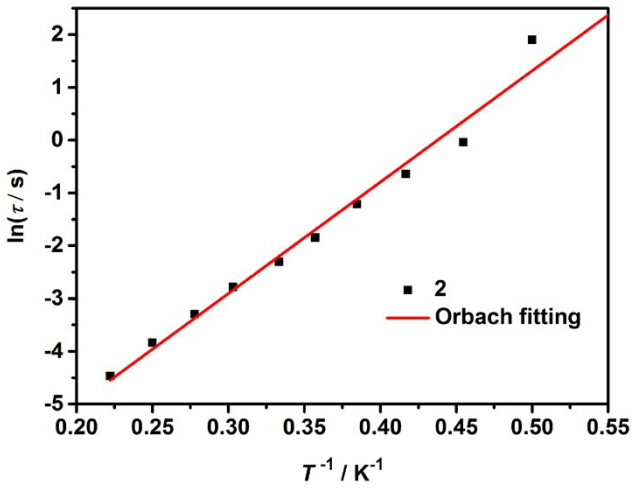

Fig. S11. Plots of ln(τ) versus T^{-1} for **2** fitted by the generalized Debye model for a one-relaxation process.

Table S7. Best fitted parameters of the Cole-Cole plots for **2**.

Temperature	χ_T	χ_S	τ	α
2.0	55.28092	-0.76679	6.70733	0.7485
2.2	38.58582	-0.39122	0.9593	0.72029
2.4	32.79391	-0.25704	0.52695	0.71194
2.6	27.81003	-0.14482	0.29797	0.70434
2.8	23.45952	0.07014	0.15772	0.68601
3.0	20.57123	0.16644	0.09979	0.67653
3.3	17.76428	0.25563	0.06196	0.6666
3.6	15.48172	0.44067	0.03709	0.64436
4.0	13.36129	0.48576	0.02163	0.63773
4.5	11.1166	0.57024	0.01145	0.62262

Table S8. The energy barriers for this work and the previously reported Dy-containing POM-based SMMs.

Compound	U_{eff}/k_B (K)	ref
$[Dy(H_2O)(Hpic)_3][Dy(Hpic)_2(\alpha_2\text{-}P_2W_{17}O_{61})]^{4-}$	119.38	3
$[N(CH_3)_4]_5H_4[Dy(\alpha\text{-}PW_{11}O_{39})_2]^{2-}$	55	4
$[N\text{-}(CH_3)_4]_4H_2[\{Dy(\alpha\text{-}PW_{11}O_{39})(H_2O)_3\}_2]^{2-}$	57	
$[(DyOH_2)_3(CO_3)(\alpha\text{-}PW_9O_{34})_2]^{11-}$	37	
$[Dy_8(PW_{10}O_{38})_4(OH)_4(H_2O)_2(W_3O_{14})]^{26-}$	64	
$\{Dy[Mo_5O_{13}(OMe)_4(NO)]_2\}^{3-}$	50	5
$[Dy_9(CO_3)_3(ampH)_2(H_2O)_{12}(PW_{10}O_{37})_6]^{35-}$	56	6
$[(PW_{11}O_{39})_2Dy_2(OH)_2(H_2O)_2]^{10-}$	141	7
$[(PW_{11}O_{39})_2Dy_2F_2(H_2O)_2]^{10-}$	106	
$[\{(AsW_9O_{33})_3Dy_2(H_2O)_4W_4O_9(H_2O)\}_2(NH_2(CH_2PO_3)_2)]^{33-}$	99	8
$\{[Dy_4As_5W_{40}O_{144}(H_2O)_{10}(gly)_2]_3\}^{21-}$	3.9	9
$[Dy(\mu_2\text{-}OH)_2Eu(\gamma\text{-}SiW_{10}O_{36})_2]^{12-}$	73	10
$[K\subset\{(AsW_9O_{33})Dy(H_2O)_2\}_6]^{35-}$	69	11
$[Dy_2(\mu_2\text{-}OH)_2(\gamma\text{-}SiW_{10}O_{36})_2]^{12-}$	66	12
$[Dy_4(Sb_3O_2)_2(SbW_{10}O_{37})_2(SbW_8O_{31})_2(H_2O)_6]^{18-}$	58.2	13
$[Dy_3(H_2O)_6Sb^{V}(H_2O)(W_3O_{11})(B\text{-}\alpha\text{-}SbW_9O_{33})_3]^{17-}$	20.1	This work

References

1 J.-C. Liu, J.-W. Zhao and Y.-F. Song, 1-D Chain Tungstotellurate Hybrids Constructed from OrganicLigand-Connecting Iron-Lanthanide Heterometal Encapsulated Tetrameric Polyoxotungstate Units. *Inorg. Chem*. 2019, **58**, 9706-9712.

2 Y. Wang, J. Lu, X. Ma, Y. Niu, V. Singh, P. Ma, C. Zhang, J. Niu and J. Wang, Synthesis, characterization and catalytic oxidation of organosilanes with a novel multilayer polyoxomolybdate containing mixed-valence antimony. *Mol Catal*. 2018, **452**, 167-174.

3 X. Wang, Y. Liu, M. Jin, Y. Wu, L. Chen and J.-W. Zhao, Two Families of Rare-Earth-Substituted Dawson-type Monomeric and Dimeric Phosphotungstates Functionalized by Carboxylic Ligands. *Cryst. Growth Des*. 2017, **17**, 5295-5308.

4 P. Ma, F. Hu, D. Zhang, C. Zhang, J. Niu and J. Wang, Magnetoluminescent Bifunctional Dysprosium-Based Phosphotungstates with Synthesis and Correlations between Structures and Properties. *Cryst. Growth Des*. 2017, **17**, 4, 1947–1956.

5 S. She, C. Gao, K. Chen, A. Bayaguud, Y. Huang, B.-W. Wang, S. Gao and Y. Wei, A Series of Weakley-type Polyoxomolybdates: Synthesis, Characterization, and Magnetic Properties by a Combined Experimental and Theoretical Approach. *Inorg. Chem*. 2018, **57**, 963-969.

6 Y. Huo, Y.-C. Chen, S.-G. Wu, J.-H. Jia, W.-B. Chen, J.-L. Liu and M.-L. Tong, pH-Controlled Assembly of Organophosphonate-Bridged Dysprosium(III) Single-Molecule Magnets Based on Polyoxometalates. *Inorg. Chem*. 2018, **57**, 6773-6777.

7 Y. Huo, Y.-C. Chen, S.-G. Wu, J.-L. Liu, J.-H. Jia, W.-B. Chen, B.-L. Wang, Y.-Q. Zhang and M.-L. Tong, Effect of Bridging Ligands on Magnetic Behavior in Dinuclear Dysprosium Cores Supported by Polyoxometalates. *Inorg. Chem*. 2019, **58**, 1301-1308.

8 Y. Huo, R. Wan, P. Ma, J. Liu, Y. Chen, D. Li, J. Niu, J. Wang and M.-L. Tong, Organophosphonate-Bridged Polyoxometalate-Based Dysprosium(III) Single-Molecule Magnet. *Inorg. Chem*. 2017, **56**, 12687-12691.

9 C. Ritchie, M. Speldrich, R. W. Gable, L. Sorace, P. Kögerler and C. Boskovic, Utilizing the Adaptive Polyoxometalate $[As_2W_{19}O_{67}(H_2O)]^{14-}$ To Support a Polynuclear Lanthanoid-Based Single-Molecule Magnet. *Inorg. Chem*. 2011, **50**, 7004-7014.

10 R. Sato, K. Suzuki, M. Sugawa and N. Mizuno, Heterodinuclear Lanthanoid-Containing Polyoxometalates: Stepwise Synthesis and Single-Molecule Magnet Behavior. *Chem. Eur. J*. 2013, **19**, 12982-12990.

11 Y. Huo, Y.-C. Chen, J.-L. Liu, J.-H. Jia, W.-B. Chen, S.-G. Wu and M.-L. Tong, A wheel-shaped Dy(iii) single-molecule magnet supported by polyoxotungstates. *Dalton Trans*. 2017, **46**, 16796-16801.

12 K. Suzuki, R. Sato and N. Mizuno, Reversible switching of single-molecule magnet behaviors by transformation of dinuclear dysprosium cores in polyoxometalates. *Chem. Sci*. 2013, **4**, 596-600.

13 J. Cai, R. Ye, K. Jia, X. Qiao, L. Zhao, J. Liu and W. Sun, pH-controlled construction of lanthanide clusters from lacunary polyoxometalate with single-molecule magnet behavior. *Inorg. Chem. Commun*, 2020, **112**, 107694.